

## Kinetic Monte Carlo Study of Triplet-Triplet Annihilation in Conjugated Luminescent Materials

Rishabh Saxena,<sup>1</sup> Tobias Meier,<sup>1</sup> Stavros Athanasopoulos,<sup>2</sup> Heinz Bässler,<sup>3</sup> and Anna Köhler<sup>1,3,\*</sup>

<sup>1</sup>*Soft Matter Optoelectronics and Bavarian Polymer Institute (BPS), University of Bayreuth, Universitätsstr. 30, 95440 Bayreuth, Germany*

<sup>2</sup>*Departamento de Física, Universidad Carlos III de Madrid, Avenida Universidad 30, 28911 Leganés, Madrid, Spain*

<sup>3</sup>*Bayreuth Institute of Macromolecular Research (BIMF), University of Bayreuth, Universitätsstr. 30, 95440 Bayreuth, Germany*



(Received 25 June 2020; accepted 17 August 2020; published 18 September 2020)

It is well known that in organic solids the collision of two excitons can give rise to delayed fluorescence (DF). Revived interest in this topic is stimulated by the current endeavor towards the development of efficient organic optoelectronic devices such as organic light-emitting diodes (OLEDs) and solar cells, or sensitizers used in photodynamic therapy. In such devices, triplet excitations are ubiquitously present but their annihilations can be either detrimental, e.g., giving rise to a roll-off of intensity in an OLED, or mandatory, e.g., if the sensitizer relies on up-conversion of long-lived low-energy triplet excitations. Since the employed materials are usually noncrystalline, optical excitations migrate via incoherent hopping. Here, we employ kinetic Monte Carlo simulations (KMC) to study the complex interplay of triplet-triplet annihilation (TTA) and quenching of the triplet excitations by impurities in a single-component system featuring a Gaussian energy landscape and variable system parameters such as the length of the hopping sites, i.e., a conjugated oligomer, the morphology of the system, the degree of disorder ( $\sigma$ ), the concentration of triplet excitations, and temperature. We also explore the effect of polaronic contributions to the hopping rates. A key conclusion is that the DF features a maximum at a temperature that scales with  $\sigma/k_B T$ . This is related to disorder-induced filamentary currents and thus locally enhanced triplet densities. We predict that a maximum for the TTA process near room temperature or above requires typically a disorder parameter of at least 70 meV.

DOI: [10.1103/PhysRevApplied.14.034050](https://doi.org/10.1103/PhysRevApplied.14.034050)

### I. INTRODUCTION

Triplet-triplet annihilation (TTA) plays an important role in controlling the operation of organic optoelectronic devices such as organic light-emitting diodes (OLEDs), organic solid-state lasers, and organic solar cells (OSCs) [1–5]. In OLEDs, TTA is devised as one of the efficient ways of converting the dark triplet excitons into emissive singlet excitons, which can decay radiatively to contribute to delayed fluorescence (DF) [6,7]. In solar cells, TTA can also be employed to improve efficiencies. The maximum theoretical power-conversion efficiency (PCE) of single-junction solar cells is dictated by the Shockley-Queisser limit, which depends on the bandgap of the light-absorbing material. TTA sensitized photon up-conversion can increase the PCE of OSCs by converting the low-energy photons into high-energy radiations that can be utilized by the absorber [8,9]. The same mechanism is used for sensitizing

semiconductor photocatalysts using the broad-spectrum sunlight [10,11]. TTA sensitized photon up-conversion is also advantageous in the fields of biomedical applications such as photoinduced drug delivery and photodynamic therapy [12,13]. In particular, up-conversion of red light with increased penetration in biological systems into blue light that is required for most photochemical reactions has been proved to be highly relevant [14].

TTA involves the collision of two triplets and thus depends on the diffusivity of triplet excitons [6,7,15–17]. Therefore, from a theoretical viewpoint, studying TTA in a model system also contributes to the fundamental understanding of triplet transport. The transport of neutral excitations through the inhomogeneously disordered medium such as an amorphous organic semiconductor film proceeds via incoherent hopping between the localized sites [18]. In this scenario, the transport is controlled by the electronic coupling between the constituent molecular units and the static disorder present due to different possible configurations of the constituent molecules [19]. The electronic coupling for spin-triplet excitations in

\*anna.koehler@uni-bayreuth.de

purely organic materials is dominated by exchange interaction (Dexter-type transfer), which depends on the wavefunction overlap [20]. Thus, the understanding developed in the process of investigating TTA can be utilized to control the triplet diffusion in order to optimize the efficiency of organic semiconductor devices extending from next-generation thermally activated delayed-fluorescence OLEDs [21] to phosphorescent-sensitizer-employed OSCs [22].

In phosphorescent OLEDs or TADF-based OLEDs made with host-guest systems, TTA is considered as one of the principle contributors towards the efficiency roll-off at high luminance [21,23,24]. Another main factor determining the efficiency roll-off in OLEDs is triplet-polaron quenching, which again depends on the diffusion of triplet excitons [25,26]. However, TTA does not necessarily need to be detrimental. It can also enhance the internal quantum efficiency of OLEDs when it contributes to delayed fluorescence via an up-conversion mechanism [27–29]. This requires efficient bimolecular recombination whereas monomolecular quenching of triplets at trap sites needs to be avoided [30,31]. Thus, in summary, TTA can be useful for solar energy conversion, photodynamic therapy, and understanding of triplet diffusivity and for the efficiency of OLEDs, and numerous studies have been devoted to improving these processes [9,13,32]. Nevertheless, a comprehensive study on how the bimolecular annihilation and monomolecular quenching processes compete with each other and the influence of material and film properties in controlling and modifying this competition is still lacking. We, therefore, intend to address this issue for a single-component system through our study.

We report an investigation of triplet hopping by means of kinetic Monte Carlo (KMC) simulations. In particular, we study the interplay between bimolecular TTA and monomolecular quenching processes (at trap sites) to eventually simulate the temperature dependence of quenching, delayed fluorescence, and phosphorescence (Ph) efficiency in conjugated polymers. Our simulation results are in agreement with the experimental observations of Hoffmann *et al.* [30]. In that paper, the authors studied the temperature dependence of Ph and DF in a series of poly(*p*-phenylene) derivatives and analyzed the findings on the basis of conventional rate equation for triplet excitons under steady-state conditions, yet only in the limit of low excitation intensities. KMC simulations provide the additional advantage of elucidating the temperature activation of the trap-induced quenching processes, which is difficult to do experimentally. When recording the phosphorescence intensity as a function of temperature, we can only observe that the Ph reduces, yet without direct indication of which fraction of this was caused by TTA, by trap-induced quenching, or by other thermally activated nonradiative decay channels. Moreover, with the

KMC simulations, we can disentangle the effect of each individual material parameter on the temperature dependence of various photophysical processes. Therefore, we use Monte Carlo simulations to determine which material properties need to be tuned to obtain minimum quenching and maximum DF at room temperature.

The simulation parameters are the degree of electronic coupling between the hopping sites, the static energetic disorder and the quencher (“trap”) concentration. Conjugated segments are designed, and the delocalization effects associated with the conjugated polymers are studied in terms of the length of the conjugated chromophores and anisotropic triplet hopping rates. Athanasopoulos *et al.* [33] showed in a KMC study of the temperature dependence of spectral diffusion that triplet transport could be affected by the number of available energetic sites for hopping because of the short-range nature of the exchange coupling. In a realistic film, polymer chains may be more or less rigid and entangled or partially aligned, so that the resulting morphology is complex. Two limiting real morphologies is one where all chains are aligned and one where all chains cross each other heavily. We try to realize these two limiting cases in our model through two design morphologies, referred to as parallel and grid lattice. In both cases, the polymer chains are taken as a rigid one-dimensional sequence of lattice sites. For the parallel lattice, the chain orientation is the same in each layer, whereas for the grid lattice, the chain orientation is rotated by 90° between alternate layers. As detailed in the methods section, this results in a significantly higher number of nearest neighbors for the grid lattice. In this way, we investigate the role of morphology in controlling the interplay between bimolecular TTA and monomolecular quenching processes. Furthermore, Miller-Abrahams triplet hopping rates only include the disorder contribution to triplet diffusion. It does not take into consideration the polaronic effects associated with the conformational distortions upon energy transfer, described in terms of the geometric reorganization energy. These polaronic effects can be incorporated by including an activation energy in the triplet hopping rates through Marcus-type formalism [34,35]. We discuss in detail how the presence of reorganization energy effects does alter the temperature dependence of mono and bimolecular processes.

This paper is structured as follows. The details of the simulation technique are given in Sec. II. The results section, Sec. III, is concerned with analyzing the influence of morphology, defects, excitation density, wavefunction delocalization, energetic disorder, and geometric relaxation energy. We also focus on comparing our KMC results to what is expected from solving rate equations. In the concluding discussion, Sec. IV, we discuss how parameters need to be tuned to obtain a high TTA yield at room temperature while summarizing our key findings.

## II. SIMULATION TECHNIQUE

The dynamic interplay of triplet-triplet annihilation and quenching of triplets at trap sites has been studied by employing a lattice-based kinetic Monte Carlo method to monitor the motion of excitons as hopping events. To describe the diffusion of triplet states through the disordered medium, we initially consider a Miller-Abrahams-(MA) type hopping between energetically uncorrelated sites of a point lattice [36]. This corresponds to a single-phonon-assisted tunneling between two sites of energy  $\varepsilon_i$  and  $\varepsilon_j$  with a rate

$$k_{ij,T} = \begin{cases} v_0 e^{-2\gamma R_{ij}}, & \varepsilon_i \geq \varepsilon_j, \\ v_0 e^{-2\gamma R_{ij}} e^{-(\varepsilon_j - \varepsilon_i)/k_B T}, & \varepsilon_i < \varepsilon_j. \end{cases} \quad (1)$$

$v_0$  is the attempt-to-hop frequency,  $\gamma$  is the inverse localization length,  $R_{ij}$  is the hopping distance, and  $k_B T$  the thermal energy. The absolute value of  $\gamma$  determines the localization of the triplet (or charge) wave function; small  $\gamma$  implies a large delocalization. The exponential decrease of the hopping rate with  $\gamma R_{ij}$  incorporates the short-range nature of the MA rate. The MA model assumes that the Boltzmann factor is equal to 1 for a downward hop, whereas thermal activation is required for a hop to a higher-energy site. The attempt-to-hop frequency is typically of the order of a phonon mode, here we choose  $v_0 = 10^{12} \text{ s}^{-1}$ . The minimum hopping time is defined by  $t_0 = (1/v_0)e^{2\gamma\alpha}$ , where  $\alpha$  is the lattice spacing (minimum hopping distance). The triplet lifetime ( $\tau_T$ ) is described as a multiple of  $t_0$  and is defined in such a way that  $(1/k_{\text{ISC}}\tau_{\text{Ph}}) \approx (\tau_T/t_0)$ , where  $k_{\text{ISC}}$  and  $\tau_{\text{Ph}}$  are the inter-system crossing (ISC) rate and phosphorescence lifetime, respectively.

While the triplets and charges are taken to diffuse only via exchange interaction [18,20,37], which depends upon the wave-function overlap, singlet excitons can also diffuse by long-range dipole interaction. Thus, to model singlet diffusion, we consider a MA + Förster-type rate:

$$k_{ij,S} = \begin{cases} \left[ v_0 e^{-2\gamma R_{ij}} + \frac{1}{\tau_s} \left( \frac{R_F}{R_{ij}} \right)^6 \right], & \varepsilon_i \geq \varepsilon_j, \\ \left[ v_0 e^{-2\gamma R_{ij}} + \frac{1}{\tau_s} \left( \frac{R_F}{R_{ij}} \right)^6 \right] e^{-(\varepsilon_j - \varepsilon_i)/k_B T}, & \varepsilon_i < \varepsilon_j. \end{cases} \quad (2)$$

$\tau_s$  is the intrinsic lifetime of singlet exciton and  $R_F$  is the Förster radius.  $\gamma$  is assumed to be the same for singlets and triplets. Here we consider  $\tau_s = 1 \text{ ns}$  and  $R_F = 3 \text{ nm}$  [38,39].  $R_F$  depends on the spectral overlap of the absorption spectrum of the acceptor and emission spectrum of the donor and is defined such that at the Förster radius the energy-transfer rate is equal to the sum of radiative and nonradiative decay rates. Dipole coupling is usually dominant over exchange coupling but in the case where the long-range Coulombic rate is very small (large  $\tau_s$  or small  $R_F$ ),

as discussed below for the triplets, the Förster rate becomes less than the Dexter rate and the short-range exchange mechanism becomes the dominant diffusion mechanism for singlets as well.

For host-guest systems, the Eindhoven group have investigated the diffusion of triplets in detail by using transient PL measurements coupled with KMC simulations, and have analyzed the relative contribution of single-step Förster-type triplet-triplet interactions and the multi-step triplet diffusion processes to the mechanism of TTA in phosphorescent host-guest systems [1,32,40–43]. The results from the Eindhoven group stimulated us to consider the contribution of dipole-dipole-coupling-induced long-range Förster rate to the triplet hopping in addition to the short-range Dexter rate [1,40–42]. The impact of increasing the Förster contribution to triplet transport on the temperature dependence of quenching, DF and Ph events is shown in Fig. S1 (see the Supplemental Material [44]). The data are shown for purely Dexter-type rates and for increased contribution from the Coulombic interactions represented by the increase in Förster radius from 1 to 5 nm. No significant changes are observed with the incorporation of Förster rates. The reason lies in the comparatively long lifetime of the triplet states. The Förster-type transfer rate is inversely proportional to the lifetime of the state considered. Thus, for triplet states, the Förster-type energy rate is rather low, so that it cannot compete with the Dexter-type energy-transfer rate. As a result, the Dexter transfer dominates the energy-transfer process entirely here. This is different from the case of strongly phosphorescent emitters that are characterized by a much shorter triplet lifetime. We, therefore, subsequently only considered the Dexter-type MA rate for the triplet hopping process.

At time  $t = 0$ , random lattice sites in the simulation box ( $100 \times 50 \times 50$  lattice sites) are initialized with a predefined number of triplets in accordance with an initial triplet density  $[T_0]$ . In our simulation, the lattice points have a spacing of 1.5 nm in direction of the  $x$  and  $z$  axis, while a spacing of 1.68 nm is adopted along the  $y$  axis. This anisotropic choice is based on matching experimental conditions in previous work [18,33]. By repeating some of the simulations for an isotropic lattice configuration, we confirm that our use of a slightly anisotropic lattice does not have a significant impact on our results and conclusion (see Fig. S2 within the Supplemental Material [44]). Generating 100 triplet excitations in this simulation box corresponds to a triplet density of about  $10^{17} \text{ cm}^{-3}$ .

In addition, some of the point sites are assigned as deep trap sites (sites of significantly lower energy) based upon a trap concentration ( $c_t$ ). The triplet (singlet) energy is taken from a Gaussian distribution centered on energy  $E_T$  ( $E_S$ ) with a variance of  $\sigma_T$  ( $\sigma_S$ ) representing the static uncorrelated disorder in triplet (singlet) excited-state energies. At each Monte Carlo step each excitation can either diffuse to

a neighboring site with rate  $k_{ij,T}$  ( $k_{ij,S}$ ) or can decay radiatively with rate  $k_{R,T}$  ( $k_{R,S}$ ) or can decay nonradiatively with rate  $k_{NR,T}$  ( $k_{NR,S}$ ). Singlets can also undergo ISC (with rate  $k_{ISC}$ ) thus leading to the generation of triplets. A schematic of all the radiative and nonradiative processes considered is shown in Fig. 1(a). Exciton-exciton annihilations and triplet quenching at the trap sites are considered as on-site and instantaneous processes, i.e., if two excitons reach the same lattice site, they annihilate. Similarly, if a triplet reaches a trap site, it is quenched. The quenching rate ( $k_Q$ ) is represented as  $k_Q = k_t c_Q$ , where  $k_t$  is the triplet diffusion rate and  $c_Q$  is the effective quencher concentration, which here is simply the trap concentration ( $c_t$ ) [30]. The trap depth is taken to be 300 meV, so that detrapping is negligible [45]. An interaction between two triplets can give rise to singlets, triplets, and quintets with a statistical probability of 1/9, 3/9, and 5/9, respectively. Therefore, if the formed singlets decay radiatively, they contribute to delayed fluorescence. Quintets are generally not formed because of the high energy associated with them; thus, this event can be simply described as the scattering of two triplets. This is how triplet-triplet annihilation is executed in this “computer experiment.” Singlet-triplet annihilation (STA) and singlet-singlet annihilation (SSA) are included in the simulations, and are modeled as on-site and instantaneous processes, in a similar way as TTA. However, they eventually turn out to be negligible as compared to other emissive and exciton loss processes. There are two reasons for this: firstly, the short lifetime of singlets (in the range

of ns) prevents the buildup of a significant population that is needed for SSA or STA events. This is in contrast to triplets that live for milliseconds and so have enough lifetime to find each other as a sequence of hops. Second, the singlets (here) in the KMC simulation are generated from the TTA events, i.e., the initial singlet population is only a small fraction of the initial triplet population. Thus at low initial triplet density considered in the simulation ( $[T_0] = 10^{16} - 10^{18} \text{ cm}^{-3}$ ), the number of singlets present at any given time is rather low. These two reasons combined, the chances of a singlet encountering a triplet or another singlet are insignificant and consequently STA and SSA events are less probable as compared to TTA. This might not be true for high  $[T_0]$  (for example,  $[T_0] \geq 5 \times 10^{18} \text{ cm}^{-3}$ ) and thus the STA and SSA events may no longer be negligible.

For each excitation, the rates of the processes described are determined. For computational efficiency reasons, hops to only a fixed number of nearest neighbors are considered, that is, we took sites up to the fourth-nearest neighbor into account. For each event  $i$ , the rate  $k_i$  is calculated. For the selection of an event, firstly, for each event  $i$  the partial sum  $S_i = \sum_{\beta=1}^i k_\beta$  is calculated. A random number is drawn from the interval  $(0, k_T]$ , with  $k_T = \sum_{\beta=1}^N k_\beta$ ,  $N$  being the total number of events. From all possible events, the event  $i$  for which  $S_{i-1} < \phi k_T \leq S_i$ ,  $\phi \in (0, 1]$  holds is selected. The selected event is executed for the corresponding excitation and the simulation time is updated by the waiting time,  $\tau_w = -\ln(X)/k_T$ , where  $X$

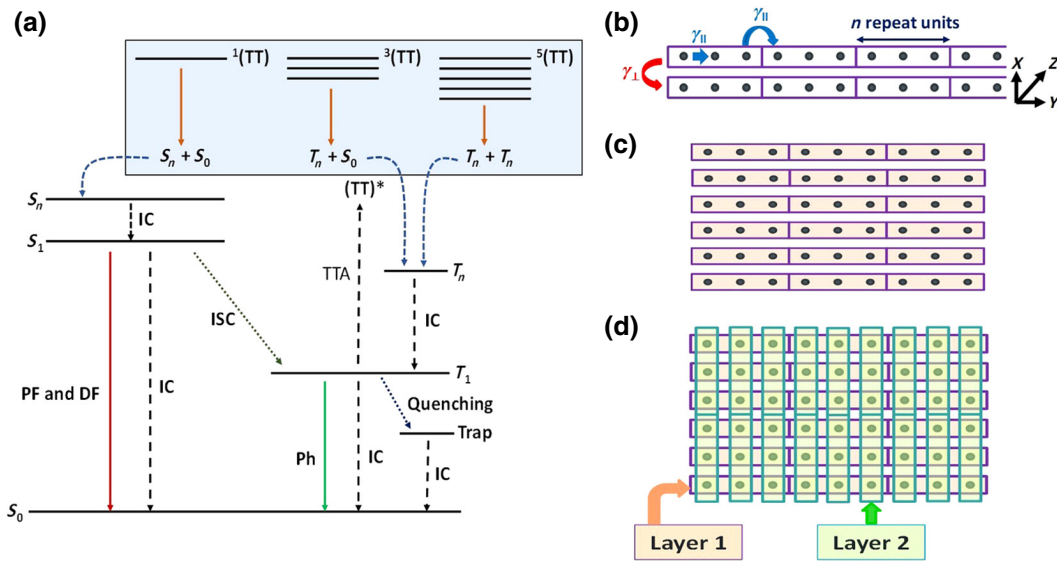


FIG. 1. (a) Schematic of all the radiative and nonradiative processes considered in the KMC simulation (PF, prompt fluorescence; DF, delayed fluorescence; IC, internal conversion; ISC, intersystem crossing; Ph, phosphorescence; TTA, triplet-triplet annihilation). The reaction of TTA can be given as  $T_1 + T_1 \rightarrow (TT)^*$ . (b) Pictorial representation of the design of a conjugated segment with “ $n$ ” isoenergetic repeat units and separate inverse localization lengths for triplet transport parallel and perpendicular to the chain. (c) Top view of the parallel lattice with all the chains along  $y$  direction in all the layers. (d) Top view of the grid lattice with all the chains in layer 1 and layer 2 aligned along  $y$  and  $x$  direction, respectively.

is a random number between 0 and 1. The simulation stops when there is no excitation left in the simulation box. Results are obtained by averaging over a sufficiently high number of trials, e.g., 100 trials (for details, refer to Sec. S1 within the Supplemental Material [44]). The effects of morphology and material parameters such as conjugation length ( $n$ ), inverse localization length along ( $\gamma_{\parallel}$ ) and perpendicular ( $\gamma_{\perp}$ ) to the chain, trap concentration ( $c_t$ ) and energetic disorder ( $\sigma$ ) on quenching, delayed fluorescence and phosphorescence processes are simulated. The resulting variation of quenching, DF and Ph events with temperature is expressed in terms of the percentage of the initial ( $t = 0$ ) number of triplets in the simulation box.

By considering extended conjugated chromophores, our study explicitly includes the effect of conjugation length. Following the approach of Athanasopoulos *et al.* we implement the delocalization of an exciton over several repeat units by defining a conjugated chromophore as a segment with “ $n$ ” isoenergetic lattice sites as illustrated in Fig. 1(b), that have strong electronic coupling between them [18,33]. The different electronic coupling for transport parallel and perpendicular to the conjugated chromophores is obtained by adopting different values for the inverse localization length  $\gamma$  if the sites  $i$  and  $j$  are in a direction parallel to the chain ( $\gamma_{\parallel}$ ) or perpendicular to the chain ( $\gamma_{\perp}$ ). Thus, the ratio  $\gamma_{\parallel} : \gamma_{\perp}$  determines the anisotropy of the triplet transport. For example,  $\gamma_{\parallel} = 1 \text{ nm}^{-1}$  and  $\gamma_{\perp} = 2 \text{ nm}^{-1}$  ( $\gamma_{\parallel} : \gamma_{\perp} = 0.5$ ) implies higher coupling in a direction parallel to the chain and lower coupling for hops perpendicular to the chain, thus making triplet hops parallel to the chain more probable than hops perpendicular to the chain. This applies to both, hops between conjugated segments of adjacent chains and hops between conjugated segments along the same chain. Moreover, since each conjugated segment is represented by a sequence of lattice points with identical energy, while the energies differ between the conjugated segments, the hops within a conjugated segment are inherently faster than the hops between the conjugated segments. This procedure allows us to treat the conjugation and delocalization effects in a stochastic manner.

When considering elongated chromophores, their mutual arrangement, i.e., the film morphology, becomes a key parameter. This is because the electronic coupling for the hopping of triplet excitons is provided by exchange interaction, which depends on the orbital overlap of the sites involved in the hopping process [Eq. (1)]. Thus, the number of accessible and adjacent neighboring sites is crucial for the transport of triplets, and for elongated chromophores, different film morphologies result in a different number of accessible neighbors. Consider, for example, a thin film consisting of elongated conjugated chromophores such as rigid oligomers that are all oriented along the same direction, e.g., along the  $y$  axis [Fig. 1(c)]. In the simplest case of such a parallel arrangement, hops are possible from

each chromophore to adjacent neighbors on either side as well as on the top and bottom and at the chromophore ends. In contrast, consider now the case where the oligomers are still all aligned along the  $y$  axis in one layer, yet they are all aligned orthogonally, e.g., along the  $x$  axis, in the layer above and below it [Fig. 1(d)]. This gridlike arrangement increases the number of contact points to next neighbors in the layer above and below from previously only two contacts in total to several contacts [for Fig. 1(d) that is two times three equal contacts in total, for the layers above and below, as illustrated in Fig. S3 within the Supplemental Material [44]]. As a consequence, more hops to sites of different energy are possible, and this significantly impacts on triplet diffusion.

The same approach was taken by Athanasopoulos *et al.* [33] who studied the temperature dependence of spectral relaxation for triplet states. They found that increasing the number of available lattice sites for hopping by changing from a parallel chromophore arrangement to a gridlike chromophore arrangement helps in overcoming local energy barriers that otherwise stop the relaxation prior to reaching lower-energy sites, in agreement with experimental results. This approach of chains in parallel or gridlike arrangement represent two extreme cases. Of course, real polymer films have far more complex morphologies and sophisticated approaches exist to represent them [46], yet our approach is sufficient to capture the essential physics with reasonable computational effort.

### III. RESULTS AND ANALYSIS

#### A. General features

In KMC simulation, we monitor the interplay between intrinsic decay of triplet excitations, i.e., phosphorescence, quenching at nonradiative scavengers (Q), and delayed fluorescence as a function of temperature and a whole set of system parameters. Figure 2(a) shows the evolution of these quantities for two lattices and for two different values of initial triplet density,  $[T_0] = 5 \times 10^{16} \text{ cm}^{-3}$  and  $10^{18} \text{ cm}^{-3}$ , equivalent to 50 and 1000 excitations, respectively. The resulting incidences are given as a percentage of the initial ( $t = 0$ ) number of triplets in the simulation box. Results for a wider range of initial triplet densities  $[T_0]$  can be found in Fig. S4 within the Supplemental Material [44]. The percentages of Ph, DF, and quenching do not add up to 100% due to the spin statistics inherent in the TTA process. Independent of the choice of lattice and excitation density, we obtain general trends that are in excellent agreement with the experimental observations of Hoffmann *et al.* [30], thus confirming our computational approach. The general evolution we observe is the following.

At very low temperature, there is phosphorescence as well as some delayed fluorescence. Upon increasing temperature, quenching turns on at the expense of Ph.

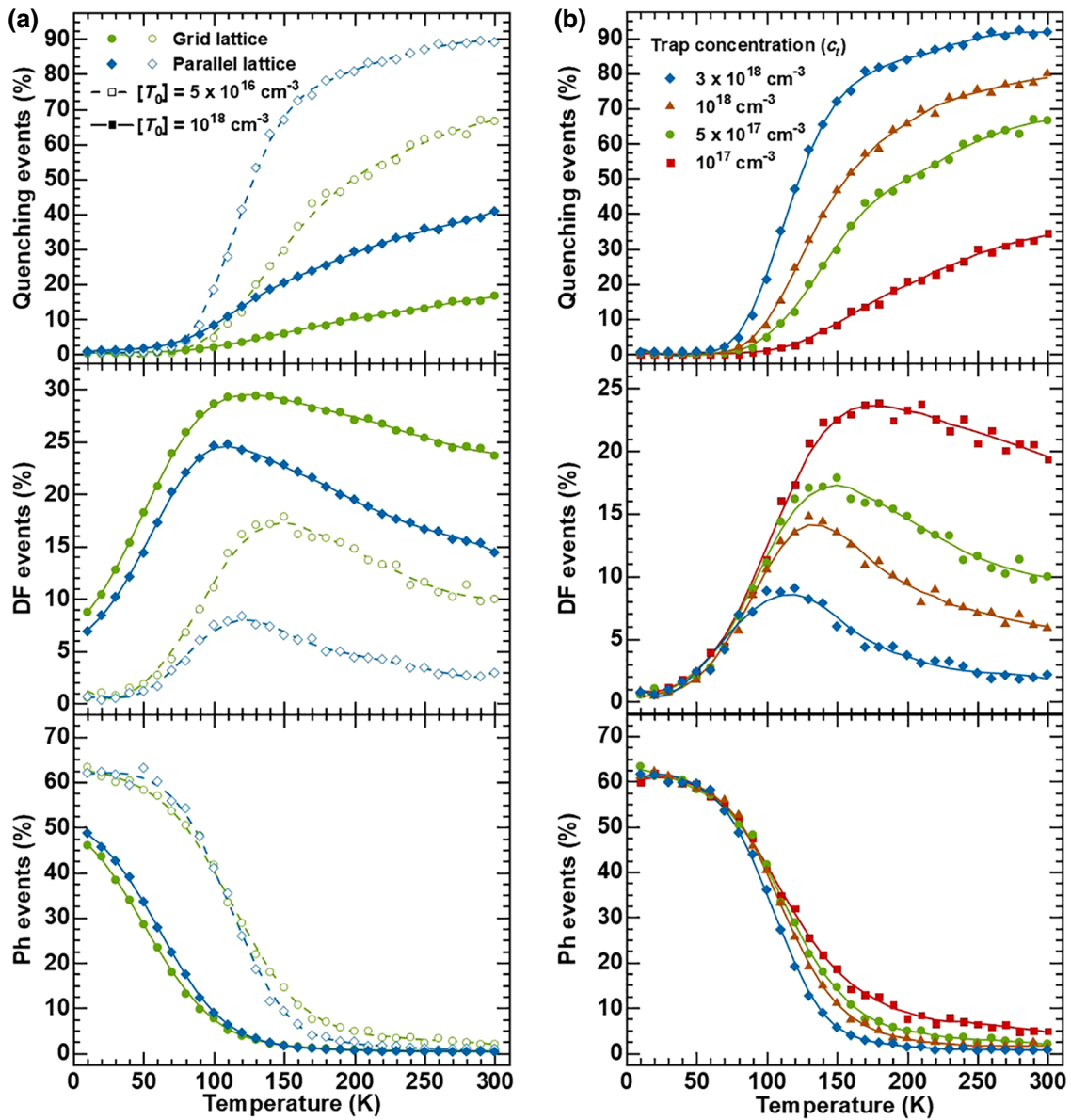


FIG. 2. Comparison of simulated quenching, DF, and Ph events (a) in the grid (green circles) and parallel lattice (blue diamonds) to study the influence of morphology on the temperature dependence of monomolecular and bimolecular recombination processes. Data are shown for two different values of initial triplet density,  $[T_0] = 5 \times 10^{16} \text{ cm}^{-3}$  (empty symbol, dashed line) and  $10^{18} \text{ cm}^{-3}$  (filled symbol, solid line). (b) With the triplet quenching rate parametrized in terms of the trap concentration ( $c_t$ ). Data for  $c_t = 10^{17} \text{ cm}^{-3}$  (red squares),  $c_t = 5 \times 10^{17} \text{ cm}^{-3}$  (green circles),  $c_t = 10^{18} \text{ cm}^{-3}$  (brown triangles), and  $c_t = 3 \times 10^{18} \text{ cm}^{-3}$  (blue diamonds). A constant coupling along and perpendicular to the chain ( $\gamma_{\parallel} = 1.5 \text{ nm}^{-1}$  and  $\gamma_{\perp} = 2 \text{ nm}^{-1}$ ) is used and a disorder of  $\sigma = 35 \text{ meV}$  is used for the triplet energy distribution. For (a),  $c_t = 5 \times 10^{17} \text{ cm}^{-3}$  and for (b) grid lattice morphology with  $n = 3$  is used. Solid lines serve as a guide to the eye.

Simultaneously DF increases such as to pass over a maximum. This behavior is a generic feature of hopping of excitations within a Gaussian density of states (DOS) distribution. At very low temperatures, most of the triplets that have been initially generated randomly within the DOS relax up to some point and subsequently emit phosphorescence [33]. At intermediate temperatures thermally activated dispersive transport leads to growing DF. At even higher temperatures, DF decreases because

the concentration of triplets needed for their bimolecular encounter is diminished due to progressive quenching at triplet scavengers.

### B. Effect of lattice choice and excitation intensity

The KMC simulations allow us to explore how the DF intensity is affected by the film morphology and the excitation density, even for high illumination intensities.

When comparing the two lattices, we observe less quenching and more DF for the grid lattice (shown in green circles). This applies not only to the peak value but, also to the value at 300 K where devices typically operate. Furthermore, the temperature  $T_{\max}$  at which the DF peaks, shifts to slightly higher values for the grid lattice. The fraction of phosphorescence events is not affected by the choice of lattice. We observe a similar trend, i.e., a reduced fraction of quenching events, more DF and, in contrast to the change of lattice, a reduction of Ph when the excitation density is increased.

The intensity dependence is straightforward to understand. For a given temperature, a higher excitation density increases the triplet population [ $T$ ], so that the bimolecular process, TTA, is favored over the monomolecular quenching process. In Fig. 2(a) we see that using a grid lattice has the same effect as increasing the excitation density, i.e., the bimolecular DF process is favored over the monomolecular quenching process. Evidently, using an arrangement with many contact points that allow for more isotropic hopping increases the chance of two triplets meeting each other, even if they have been generated at some distance and at different chains. This is consistent with the earlier results of Athanasopoulos *et al.* on spectral diffusion, where very low-energy sites in the DOS can only be reached for the grid lattice [33].

Since our primary aim is to establish guidelines for achieving high DF at room temperature, therefore we discuss the influence of all the other material parameters for the grid lattice with an initial triplet density [ $T_0$ ] of  $5 \times 10^{16} \text{ cm}^{-3}$ . This value corresponds to the triplet density generated in an optical experiment with an excitation fluence of approximately  $10 \mu\text{J}/\text{cm}^2$ , incident photon wavelength of 355 nm (typical of a Nd : YAG laser), an absorption length of 100 nm with an underlying assumption of uniform absorption with a coefficient of about  $10^5 \text{ cm}^{-1}$  throughout the film thickness and considering a singlet-to-triplet yield of about 1%–2% typical for purely organic materials (with no heavy atoms and ISC rate of approximately  $10^7 \text{ s}^{-1}$ ) [20].

### C. Influence of trap concentration ( $c_t$ )

Even well synthesized and purified compounds contain some residual amount of structural or chemical defect sites where triplet states can be quenched. It is clear that their amount plays a key role in controlling the dynamic interplay between the bimolecular and monomolecular processes. Figure 2(b) illustrates quantitatively the impact of reducing the concentration of such quenching sites. In agreement with typical defect concentrations [47], we vary the trap concentration from  $3 \times 10^{18} \text{ cm}^{-3}$  to  $10^{17} \text{ cm}^{-3}$  and observe a strong increase in the DF at room temperature as the defect concentration reduces, in addition to a slight shift of the DF peak ( $T_{\max}$ ) to higher temperatures.

Evidently, the purity of compounds is a key parameter to obtain high TTA rates.

### D. Influence of delocalization

The present OLED technology is dominated by using molecules suitable for making devices through thermal evaporation in vacuum. Nevertheless, using solution-processed molecules such as oligomers or even polymers is still a possible avenue. Moreover, triplets move by means of wave-function overlap, so that transport along a conjugated backbone is usually faster than hopping to an adjacent chromophore [18]. Therefore, conjugation of the chromophore should affect the temperature evolution of bimolecular annihilation and monomolecular quenching processes. As described above and as depicted in Fig. 1(b), in our simulation, the length of a chromophore is defined through the number of adjacent isoenergetic sites ( $n$ ) along the chain.

Figure 3(a) shows the effect of conjugation on quenching, DF and Ph events for the grid lattice. Quenching events decrease with increasing length of the conjugated segment and concomitantly, DF events increase with the peak in DF (represented by  $T_{\max}$ ) remaining at approximately similar temperature. The fraction of DF events at room temperature is also raised. This effect can be understood by the reasoning already brought forward to comprehend the increased DF for the grid morphology compared to the parallel lattice. As the length of the conjugated segment is increased, the number of crossing points to chromophores of different energies raises [cf. Fig. 1(d)]. In this way, an increasing conjugation length leads to an increased rate of successful hops to adjacent chromophores and, somewhat paradox, more isotropic diffusion. This, in turn, enhances the chance of two triplets meeting, i.e., the bimolecular recombination rate, and thus suppresses the relative number of quenching events.

The anisotropy of the excitation transport also becomes key when considering transport along the polymer chains. This anisotropy is studied by systematically varying the ratio  $\gamma_{\parallel} : \gamma_{\perp}$  as, due to the Dexter-type nature of triplet transfer, this ratio controls the directionality and hence the anisotropy of triplet diffusion [18,33].  $\gamma_{\parallel} : \gamma_{\perp} = 1$  corresponds to isotropic diffusion, whereas  $\gamma_{\parallel} : \gamma_{\perp} < 1$  ensures that coupling along the chain is stronger than perpendicular to it. Figure 3(b) summarizes this effect for a conjugated segment of length  $n = 10$ . As the hopping events perpendicular to the chain direction are increased by reducing  $\gamma_{\perp}$  from 4 to 2, we observe an increase in DF events up to about 150 K, yet there is no effect at higher temperatures. This is in contrast to the effects obtained when using the grid over the parallel-chain arrangement or when increasing the conjugation length, and, at first sight, may seem counterintuitive since increasing the electronic coupling to adjacent chains should have a similar effect. A similar

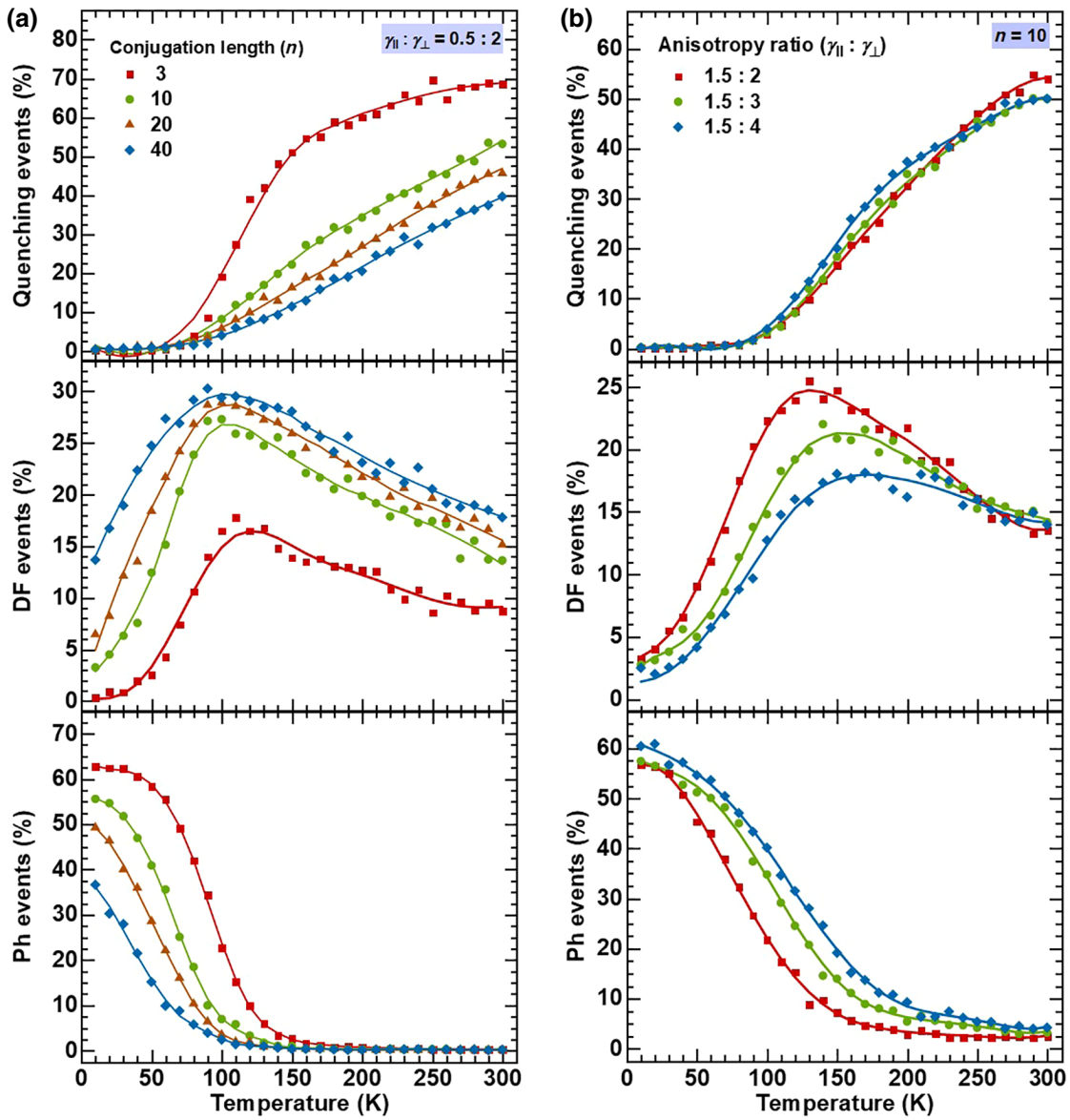


FIG. 3. Influence of delocalization is studied by simulating the number of quenching, DF, and Ph events by (a) varying the length of the conjugated segment ( $n$ ) from 3 to 40 for the grid lattice morphology with  $\gamma_{\parallel} = 0.5 \text{ nm}^{-1}$  and  $\gamma_{\perp} = 2 \text{ nm}^{-1}$  and (b) for a fixed  $n$  ( $n = 10$ ) by varying the anisotropy of coupling with a constant parallel to the chain inverse localization length of  $\gamma_{\parallel} = 1.5 \text{ nm}^{-1}$  and varying the one perpendicular to the chain ( $\gamma_{\perp}$ ) from 4 to 2  $\text{nm}^{-1}$ , thus increasing the interchain hopping transport. The results are obtained with a constant trap concentration  $c_t = 5 \times 10^{17} \text{ cm}^{-3}$  and energetic disorder  $\sigma = 35 \text{ meV}$ . Solid lines serve as a guide to the eye.

result is obtained when keeping  $\gamma_{\perp}$  constant and reducing  $\gamma_{\parallel}$  such as to increase the conjugation along the chain, see Fig. S5 within the Supplemental Material [44].

It can be easily understood by recalling that the MA rate [Eq. (1)], consists of two exponential terms, that is the strength of the electronic coupling,  $e^{-2\gamma R_{ij}}$ , and the Boltzmann factor for upward jumps. Increasing the coupling perpendicular to the chain increases the off-chain hopping rate. While this dominates from low temperatures up to about 150 K, from 150 K onwards the Boltzmann term controls the total rate, irrespective of the enhancement in

the coupling. We note that going to even smaller values than 2 for  $\gamma_{\perp}$  is unrealistic. This strong influence of the Boltzmann factor calls for a closer inspection on the impact of energetic disorder.

### E. Influence of energetic disorder ( $\sigma$ )

Figure 4(a) shows the variation of Ph, DF, and quenching events for different energetic disorder values for the triplets, using the same parameters and the MA rate employed so far. As the energetic disorder increases from

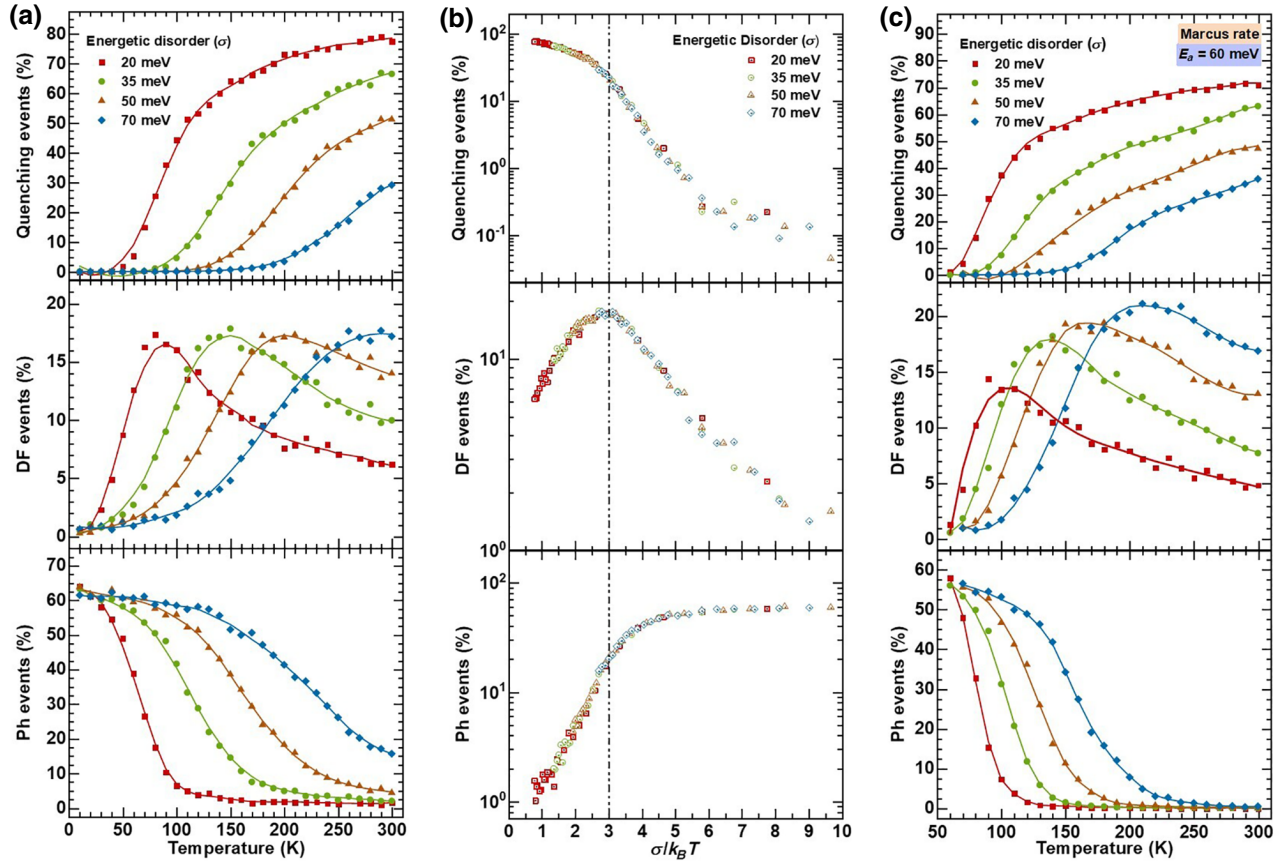


FIG. 4. Effect of static disorder ( $\sigma$ ) is investigated on the temperature dependence of quenching, DF, and Ph events for (a) and (b) Miller-Abrahams rate and (c) for a Marcus rate with  $E_a = 60$  meV. (b) shows data in (a) represented with respect to thermal energy normalized disorder ( $\sigma$ ) values instead of temperature on a semilog scale. A grid morphology with the length of the conjugated segment  $n = 3$  and a constant coupling along and perpendicular to the chain ( $\gamma_{\parallel} = 1.5 \text{ nm}^{-1}$  and  $\gamma_{\perp} = 2 \text{ nm}^{-1}$ ) is used. Trap concentration  $c_t = 5 \times 10^{17} \text{ cm}^{-3}$  is used for obtaining the simulation results. Solid lines serve as a guide to the eye.

20 to 70 meV, both TTA and quenching rates slow down and the DF peak ( $T_{\text{max}}$ ) shifts to room temperature for a disorder of 70 meV, while remaining at the same value throughout. It appears that the same curves are just stretched towards higher temperature values.

In fact, for a Gaussian DOS with a MA hopping rate, there is an inherent scalability between disorder and temperature [19,39,48,49]. This is illustrated in Fig. 4(b), where the same data are displayed on a semilogarithmic scale as a function of  $\sigma/k_B T$  instead of temperature. As shown, the quenching, DF, and Ph events for all the disorder values superimpose on each other for identical  $\sigma/k_B T$  values. In particular, the DF events peak at around  $\sigma/k_B T \approx 3$  for all the disorder values. Thus, to obtain maximum DF at room temperature (with  $k_B T \approx 25$  meV), an energetic disorder of  $\sigma \approx 75$  meV is required (for values of  $\gamma$  and trap concentration as given in the caption to Fig. 4).

## F. Influence of geometric relaxation energy ( $\lambda$ )

The MA rate is very easy to implement in a simulation, and it is thus widely used to model excitation transport in disordered materials. However, it neglects that the transfer of an excitation from one site to another is generally associated with some change in molecular configuration. The energetic changes associated with these molecular distortions are expressed in terms of the geometric relaxation energy ( $\lambda$ ) [50]. When  $\lambda$  is small compared to the site disorder parametrized through  $\sigma$ , the MA rate still gives a very good description [34,37]. We estimate this is often the case for charges, yet not for triplets, where geometric relaxation energies can be large compared to  $\sigma$ , so that they dominate the transport at room temperature [37,51]. When such electron-phonon coupling cannot be neglected, relaxation energy must also enter the expression of triplet hopping rate as an additional activation term and the transport at high temperatures can be modeled within

the Marcus formalism [35].

$$k_{ij} = \frac{J_{ij}^2}{\hbar} \sqrt{\frac{\pi}{4E_a k_B T}} \exp \left\{ -\frac{(\Delta G + 4E_a)^2}{16E_a k_B T} \right\}, \quad (3)$$

where  $J_{ij} = J_0 e^{-\gamma R_{ij}}$  represents the electronic coupling.  $J_0$  is the nearest-neighbor coupling constant.  $E_a$  represents the additional activation energy due to the geometric reorganization and relates to the reorganization energy ( $\lambda$ ) as  $E_a = \lambda/4$ .  $\Delta G = (\varepsilon_j - \varepsilon_i)$  represents the free-energy difference between the two hopping sites and thus incorporates the effect of energetic disorder ( $\sigma$ ).

We compare the influence of material parameters on TTA and quenching rate when the Marcus rate, Eq. (3), is used for triplet diffusion and summarize the differences as compared with the MA approach. We find that the influence of trap concentration ( $c_t$ ), conjugation length ( $n$ ), and anisotropy ratio ( $\gamma_{\parallel} : \gamma_{\perp}$ ) are qualitatively and quantitatively very similar to the results obtained by using Miller-Abrahams rate, as shown in Figs. S6, S7, and S8 within the Supplemental Material [44]. A quantitative difference occurs when considering the effect of energetic disorder on the temperature dependence of quenching, DF, and Ph events in the presence of geometric reorganization [Fig. 4(c)]. The activation energy is fixed at  $E_a = 60$  meV and  $\sigma$  is varied from 20 to 70 meV. Similar to the scenario when the MA rate is used, the relative influence of quenching compared to TTA is suppressed with increasing disorder so that the peak of the DF shifts to higher temperature. However, this peak shift is now accompanied by an increase in overall intensity for high disorder values, and a decrease for low disorder values. For  $\sigma$  of about 35 meV, the temperature and intensity of the DF peak are identical for the MA and the Marcus rate.

To understand the origin of this difference, we compare the effect of disorder for both the approaches (Fig. S9 within the Supplemental Material [44]). We find that the percentage of quenching events at the DF peak temperature,  $T_{\max}$ , is constant when MA rates are used, yet it reduces with increasing disorder when Marcus rates are used. More precisely, the quenching events in the Marcus case fall from values above the one for the MA case to values below it. The reason for this is related to the way how an additional activation energy impacts on the overall hopping rates given by Eqs. (1) and (3). For a MA rate, an increase in disorder can be compensated by an increase in temperature, so that the average hopping rate remains unchanged. For higher disorder, the DF peak occurs at correspondingly higher temperature, yet the ratio of quenching events to DF events at  $T_{\max}$  remains unaffected. In contrast, in the Marcus rate, Eq. (3), a constant term is added. How this impact on the rate depends on  $\sigma$  relative to  $E_a$  [34,52]. A detailed analysis is complex and requires going beyond the rate equation for two individual sites, rather, the statistical mean value for the mobility

of the triplet exciton needs to be considered, as detailed in Sec. S2 within the Supplemental Material [44]. The effect is that in the Marcus case, the mobility of triplets decreases faster with temperature when the disorder is large, compared to the MA case. As a result, at higher temperatures, quenching is more suppressed than in the MA case. Less quenching implies a higher triplet concentration [ $T$ ], and thus the bimolecular TTA process is favored. Overall, this shifts  $T_{\max}$  to lower temperatures compared to the MA case [Fig. 4(a)] and leads to higher peak values.

While variation of the disorder has a strong impact on the fraction of TTA events that occur, changes in the geometric reorganization energy do not affect the intensity of the room-temperature DF (Fig. 5). Similar to the case of varying the off-chain coupling [Fig. 3(b)], the additional activation energy due to molecular reorganization effects only modifies the low-temperature part of the curve, while the behavior at room temperature is entirely dominated by the disorder contribution.

### G. The role of disorder in the TTA process

The role of disorder is twofold. First, it changes the hopping rate, i.e., Eq. (1) or (3). Second, and perhaps less appreciated though relevant, is the fact that by changing the energy landscape, it modifies the spatial distribution of the triplet states. This is illustrated in Fig. 6 for MA rates for two cases,  $\sigma/k_B T < 1$  and  $\sigma/k_B T > 1$ . Taking  $k_B T$  at room temperature, this corresponds to  $\sigma$  values of 20 and 70 meV, respectively. Analogous figures for 35 and 50 meV can be found within the Supplemental Material [44] (Fig. S10). The color plot in Fig. 6 (heat map) indicates an exemplary cut through the  $X$ - $Z$  plane. In the top panel, the color indicates the number of annihilations that occur at any lattice site in that plane. They are normalized relative to the maximum number of annihilations observed at a lattice site in that plane. In the bottom panel, any lattice sites with energies that are more than  $1.5\sigma$  below the center of the DOS are indicated in red color. Grid lines are shown to ease visual comparison between the top and bottom panel. In addition, an enlarged view is shown in Fig. S11 within the Supplemental Material [44]. Evidently, there is little correlation between the fraction of TTA events in a lattice plane and the lower-energy sites when the disorder is smaller than the mean thermal energy. However, when the energetic landscape has valleys deeper than the mean available thermal energy, the TTA events are observed mostly in the energetic valleys. To allow for a more quantitative assessment, we calculate Pearson linear correlation function ( $\rho$ ). Essentially, this function corresponds to the covariance of the energy of the lattice sites and the number of annihilations happening at those lattice sites within a particular plane normalized by the product of their standard deviations (for expression refer to Sec. S3 within the Supplemental Material [44]). We find  $\rho = -0.12$  for a

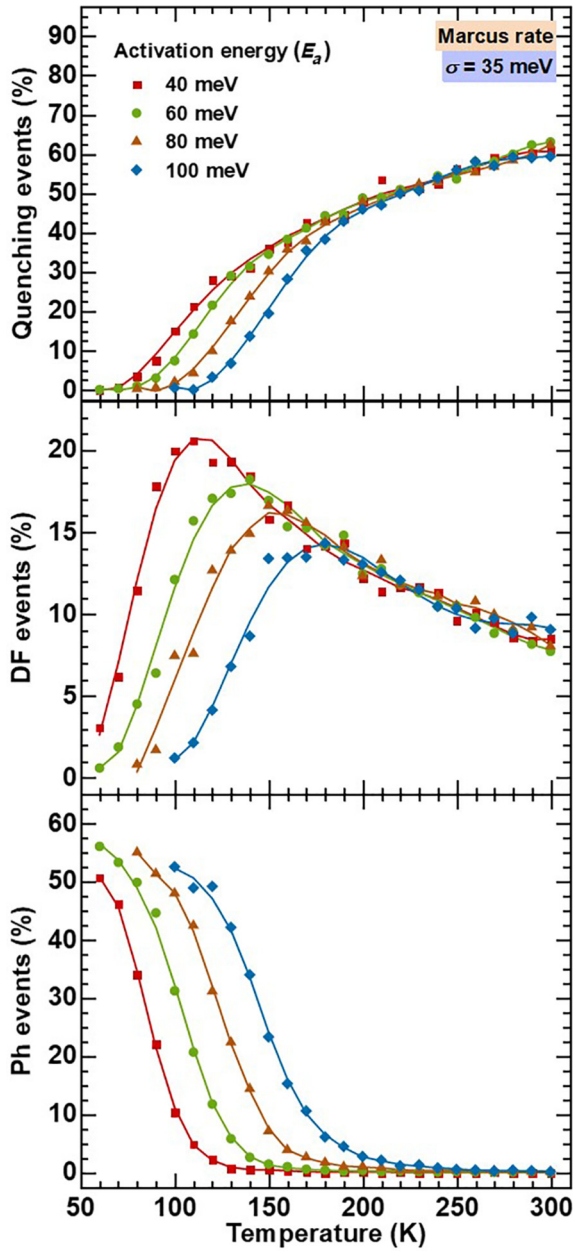


FIG. 5. Simulated dependence of quenching, DF, and Ph events with Marcus rate in the presence of both energetic disorder and reorganization induced polaronic disorder. Simulated data for energetic disorder  $\sigma = 35$  meV and  $E_a = 40, 60, 80,$  and  $100$  meV. Solid lines serve as a guide to the eye.

disorder parameter of  $\sigma = 20$  meV, yet  $\rho = -0.21, -0.23$  and  $-0.22$  for  $\sigma = 35, 50,$  and  $70$  meV. These  $\rho$  values are obtained by averaging over all the planes in the simulation box. It is negative because there is negative covariance (low energy implies a high number of annihilations).

This is straightforward to understand and can be explained in the framework of the transport energy developed for charge carriers [53]. For  $\sigma/k_B T > 1$ , the triplets

relax energetically and hop predominantly through the valleys, so that a nonuniform distribution results. Such a filamentary nature of excitation transport has previously been observed for charges in disordered materials [54,55]. As the bimolecular TTA process depends quadratically on the triplet density, the TTA events also take place predominantly in the valleys. This implies a higher effective TTA rate than is expected on the basis of the spatially averaged triplet density. Evidently, a high  $\sigma/k_B T$  value is required for a high TTA yield.

## H. Comparison to analytical calculation

It is instructive to compare the results of the MC simulation to experimental data and to analytical calculations. In earlier work, we along with others were already able to demonstrate that kinetic MC simulations can accurately reproduce the spectral signatures of triplet diffusion in conjugated materials [1,18]. Nearly a decade ago, Hoffmann *et al.* published a detailed investigation of the temperature dependence of delayed fluorescence and phosphorescence for poly- and oligofluorenes [30]. As mentioned earlier, the results of our MC simulation are in very good agreement with the experimental data by Hoffmann *et al.* In this work, Hoffmann *et al.* also formulated an analytical theory for the limit of low excitation density that could describe the experimental results, albeit only when the conjugation length was not too long. Here we extend the approach by Hoffmann *et al.* to apply to any excitation density and compare the analytical result to our KMC data.

Bimolecular recombination with an annihilation rate constant  $\gamma_{\text{TTA}}$  (not to be confused with the symbol for inverse conjugation length) gives rise to DF with an intensity

$$I_{\text{DF}} = c\gamma_{\text{TTA}}[T]^2, \quad (4)$$

where  $c$  is a constant equal to the fraction of triplet-triplet encounters that generate a singlet state times the rate constant for the radiative singlet decay.  $[T]$  denotes the concentration of triplet excitons. Under steady-state conditions

$$\frac{d[T]}{dt} = 0 = G - (k_{\text{R}} + k_{\text{NR}} + k_{\text{Q}})[T] - \gamma_{\text{TTA}}[T]^2, \quad (5)$$

where  $G$  is the formation rate of triplet excitons,  $k_{\text{R}}$  and  $k_{\text{NR}}$  are radiative and nonradiative decay rates, and  $k_{\text{Q}}$  is the monomolecular quenching rate. Solving the quadratic Eq. (5) for triplet exciton concentration and neglecting the negative solution for  $[T]$  yields

$$[T] = \frac{-(k_{\text{R}} + k_{\text{NR}} + k_{\text{Q}}) + \sqrt{(k_{\text{R}} + k_{\text{NR}} + k_{\text{Q}})^2 + 4\gamma_{\text{TTA}}G}}{2\gamma_{\text{TTA}}}. \quad (6)$$

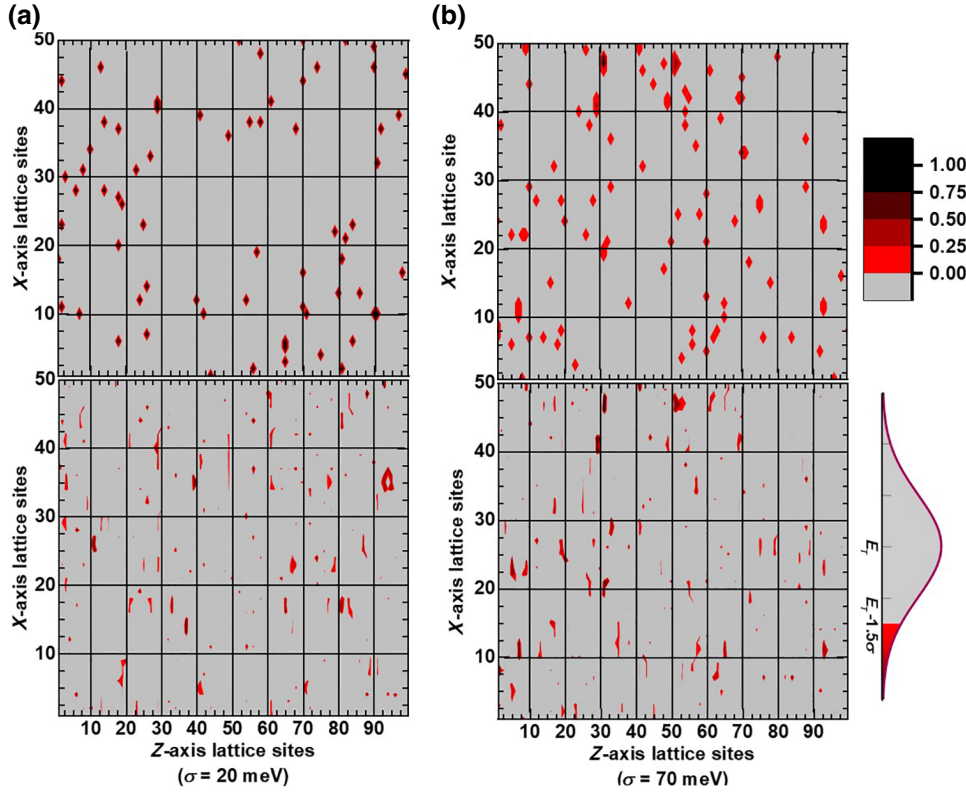


FIG. 6. Color maps showing (top panels) the relative number of annihilations per lattice site in the  $X$ - $Z$  plane (with gray indicating zero annihilations and black implying the maximum number of annihilation events found in that plane at a site), and (bottom panels) the triplet state energies for each site in that plane. Sites with energies below  $1.5\sigma$  of the mean triplet energy ( $E_T$ ) are colored in red. This is shown for 300 K for (a)  $\sigma = 20$  meV (i.e.,  $\sigma/k_B T < 1$ ) and (b)  $\sigma = 70$  meV (i.e.,  $\sigma/k_B T > 1$ ).

The condition to derive  $T_{\max}$ , the temperature at which DF exhibits a maximum.

$$\frac{\partial I_{\text{DF}}}{\partial T} = 0. \quad (7)$$

To carry out the derivative, we need to assume a temperature dependence for the different parameters involved. We take  $G$ ,  $k_R$ , and  $k_{\text{NR}}$  to be independent of temperature in agreement with usual experimental findings, while we consider  $k_Q$  and  $\gamma_{\text{TTA}}$  to vary with temperature. For simplicity, we assume an Arrheniuslike temperature dependence of  $k_Q$  and  $\gamma_{\text{TTA}}$  with constant activation energy  $E_{\text{act}}$ , viz.

$$k_Q = k_{Q0} + k_{Q1} \exp\left(\frac{-E_{\text{act}}}{k_B T}\right), \quad (8)$$

$$\gamma_{\text{TTA}} = \gamma_0 + \gamma_1 \exp\left(\frac{-E_{\text{act}}}{k_B T}\right). \quad (9)$$

Inserting Eqs. (8) and (9) into Eq. (6), Eq. (6) in Eq. (4) and then using  $I_{\text{DF}}$  from Eq. (4) into Eq. (7) and solving it, we obtain

$$T_{\max,1} = \frac{E_{\text{act}}}{k_B} \left\{ \ln \left[ \frac{\gamma_1 k_{Q1}}{\gamma_1 (k_R + k_{\text{NR}} + k_{Q0}) - 2k_{Q1} \gamma_0} \right] \right\}^{-1}, \quad (10)$$

$$T_{\max,2} = \frac{E_{\text{act}}}{k_B} \left[ \ln \left( \frac{-\gamma_1}{\gamma_0} \right) \right]^{-1}. \quad (11)$$

In Eq. (9)  $\gamma_0$  and  $\gamma_1 > 0$ , so that  $T_{\max,2}$  is not a proper solution in this context. Thus  $T_{\max} = T_{\max,1}$ . This is, exactly the same expression that was obtained by Hoffmann *et al.* in the limit of low exciton concentration by neglecting the quadratic triplet-triplet annihilation term in Eq. (5). As shown by Hoffmann for the low-intensity case, a similar expression results when the argument ( $E_{\text{act}}/k_B T$ ) in the exponential of Eqs. (5) and (6) is replaced by  $(\sigma/k_B T)^2$ , that is

$$T_{\max,1} = \frac{\sigma}{k_B} \left\{ \ln \left[ \frac{\gamma_1 k_{Q1}}{\gamma_1 (k_R + k_{\text{NR}} + k_{Q0}) - 2k_{Q1} \gamma_0} \right] \right\}^{-1/2}. \quad (12)$$

Equations (10) and (12) reflect the dependence of  $T_{\max}$  on key parameters such as the sample purity and on the energetic disorder. The central observation is, however, that  $T_{\max}$  does not contain any dependence on the generation rate  $G$ . This is at variance with the simulation results (cf. Fig. 1 and S4) as well as with the experimental observations. Both indicate a dependence of DF peak position on the excitation intensity. Thus, we reach the conclusion that the constants  $k_{Q0}$ ,  $k_{Q1}$ ,  $\gamma_0$ , and  $\gamma_1$  as described in Eqs. (8) and (9) must, in some way, be dependent on the generation intensity.

This information is key and needs to be included to correctly predict the dependence of DF on the excitation intensity. In contrast to analytical calculations, MC simulations inherently consider the excitation intensity dependence of different emissive processes and exciton-loss processes. In addition, any time dependence of the diffusion and annihilation processes is inherently included, while analytical calculations (described above) represent the steady-state condition [56]. The energetic relaxation and subsequent diffusion of excitations into the valleys of the energy landscape is well known [54,57]. This enhances the local triplet density there over the average value. We consider this nonuniform triplet density to be the reason for the dependence of the above constants on the generation rate  $G$ . [Comparison to the MC simulations in Figs. 3 and 4 with Eq. (10) further show that the dependence of  $T_{\max}$  on conjugation length and transport anisotropy is also not captured by Eq. (10), unless the impact of conjugation length and transport anisotropy on the constants  $k_{Q0}$ ,  $k_{Q1}$ ,  $\gamma_0$  and  $\gamma_1$  are explicitly taken into account. This is, though, of lesser relevance since this dependence is comparatively weak, as evident in Figs. 3 and 4.]

#### IV. CONCLUDING DISCUSSION

One of the advantages of kinetic MC simulations is that it allows to decouple the effects caused from different material parameters by systematically varying only one of them. In this way, our study allowed us to identify and highlight the strong role of detrimental triplet quenching by impurities. Further, we find that the film morphology plays a key role in determining the relative extent of bimolecular and monomolecular recombination. A morphology of mostly parallel chains, conducive for directional transport, favors quenching at the trap sites whereas a gridlike morphology of many crossing chains that allows for more isotropic hopping enhances the fraction of TTA events. Our study of delocalization effects suggests that increasing the length of conjugated segments improves DF by raising the number of readily accessible crossing points to other chains, thus increasing the isotropy of transport.

The role of energetic disorder is twofold. First, an increased disorder reduces the triplet diffusivity [19,39,48]. A high diffusivity enables triplet motion to impurity sites where their concentration is reduced. Since TTA depends quadratically on the triplet concentration, the fraction of TTA events eventually reduces. Thus, a moderately low triplet diffusivity is desirable. In fact, in our earlier study we found that the reason why the number of TTA events peaks at a certain temperature is simply that the temperature activated diffusivity becomes too high [30]. This is consistent with the results of Blom and co-workers on singlet diffusion in poly-(*p*-phenylene vinylene) (PPV) derivatives [58]. They found that the more disordered super-yellow-PPV had a lower diffusivity at

room temperature and thus a longer exciton lifetime. This gives rise to a higher photoluminescence quantum yield due to the slower exciton diffusion towards quenching sites [59].

The second role of energetic disorder, however, is that it causes filamentary transport, thus enhancing the probability of two triplets to encounter each other rather than an impurity. A key result of our study is that energetic disorder is crucial for obtaining a high yield of TTA events at room temperature. For typical values of the remaining parameters, a disorder in the order of  $\sigma/k_B T \approx 3$  is required to obtain a DF peak at room temperature. Using values such as  $\sigma \approx 70$  meV, a trap concentration of approximately  $10^{17}$  cm<sup>-3</sup>,  $\gamma_{\parallel} = 0.5$  nm<sup>-1</sup>,  $\gamma_{\perp} = 2$  nm<sup>-1</sup> and a conjugation length of 20 repeat units, we obtain a yield of TTA events of 140%, i.e., about 30% DF events for an excitation intensity of  $5 \times 10^{16}$  cm<sup>-3</sup> (Fig. S12 within the Supplemental Material [44]). We note that the yield of TTA events exceeds 100% of the initial number of triplets present. This is because through the spin statistics, we consider secondary processes, i.e., that two triplets may collide to form one TTA event, then separate (e.g., because they formed a quintet state), and collide again with a certain probability.

We finally address the question of modeling excitation transport via the energetic-disorder-controlled Miller-Abrahams or polaronic-activation-controlled Marcus approach, which has always been a topic of debate in the community [60]. Coehoorn and co-workers have been able to successfully model charge transport and exciton dynamics in OLEDs by simply incorporating the Miller-Abrahams transport rates [1,32,40–42]. The recent full quantum treatment of charge-carrier dynamics in amorphous organic semiconductors indeed confirms that the MA approach captures the salient features of transport, albeit at low temperatures [61]. In our earlier studies we observed that the reorganization energy can have a substantial influence on the rates for triplet processes, notably at higher temperatures ( $>100$  K), which requires the use of the Marcus rate to describe the hopping process [18]. Therefore, we use the MA approach to first address the current problem and subsequently only highlighted the key differences that can be expected if the reorganization energy effects are explicitly considered in these energetically disordered materials. We observe that delocalization effects and the effects due to trap concentration do not change. Disorder effects are also more or less similar except for an increase in DF intensity for higher energetic disorders. Decreased reorganization energy increases the DF at low temperatures but does not have any effect on room-temperature DF. We attribute the comparatively low sensitivity of the result to the specific hopping rate chosen to the fact that this study is concerned with determining yields for triplet processes rather than rates.

In brief, we develop a kinetic Monte Carlo study that describes how TTA, triplet quenching and phosphorescence evolve as a function of temperature when a wide range of experimental and material parameters are varied. Our results are qualitatively consistent over a whole range of parameters with the experiments performed on a series of poly(*p*-polyfluorenes), confirming the suitability of the model [33]. We find that the choice of hopping rate is not critical when considering the yield of TTA events, and that analytical studies need to include the intensity and time dependence of quenching and annihilation constants to come to a description that reflects experiments. Optimizing the TTA process, and concomitantly the yield of DF, to peak at room temperature is possible. It requires (i) a high disorder and therefore dispersive transport (in the range of  $\sigma/k_B T \approx 3$ ), (ii) a high sample purity (about  $10^{17}$  quenching sites per  $\text{cm}^3$ ), and (iii) a morphology and conjugation length with many contact points that enables isotropic hopping.

### ACKNOWLEDGMENTS

We acknowledge funding from the Deutsche Forschungsgemeinschaft, Sachbeihilfe “Triplettkonzepte für Organische Photovoltaik: neue Materialien, Solarzellen und Mechanismen“, as well as through the Marie Skłodowska-Curie Actions (MSCA) via the Innovative Training Network (ITN) TADFlife (GA 812872). This work is also supported by the Universidad Carlos III de Madrid, the European Union’s Seventh Framework Programme for research, technological development and demonstration under Grant Agreement No. 600371, el Ministerio de Economía, Industria y Competitividad (COFUND2014-51509), el Ministerio de Educación, cultura y Deporte (CEI-15-17), Banco Santander and el Ministerio de Ciencia, Innovación y Universidades (RTI2018-101020-B-I00).

- 
- [1] H. van Eersel, P. A. Bobbert, and R. Coehoorn, Kinetic Monte Carlo study of triplet-triplet annihilation in organic phosphorescent emitters, *J. Appl. Phys.* **117**, 115502 (2015).
- [2] C. Gärtner, C. Karnutsch, U. Lemmer, and C. Pflumm, The influence of annihilation processes on the threshold current density of organic laser diodes, *J. Appl. Phys.* **101**, 023107 (2007).
- [3] A. Monguzzi and J. Pedrini, Recent advances in the application triplet-triplet annihilation-based photon upconversion systems to solar technologies, *J. Photonics Energy* **8**, 1 (2017).
- [4] D. W. Gehrig, I. A. Howard, and F. Laquai, Charge carrier generation followed by triplet state formation, annihilation, and carrier recreation in PBDTTT-C/PC60BM photovoltaic blends, *J. Phys. Chem. C* **119**, 13509 (2015).
- [5] P. C. Chow, S. Gelinas, A. Rao, and R. H. Friend, Quantitative bimolecular recombination in organic photovoltaics through triplet exciton formation, *J. Am. Chem. Soc.* **136**, 3424 (2014).
- [6] S. Balushev, T. Miteva, V. Yakutkin, G. Nelles, A. Yasuda, and G. Wegner, Up-conversion Fluorescence: Noncoherent Excitation by Sunlight, *Phys. Rev. Lett.* **97**, 143903 (2006).
- [7] F. Laquai, G. Wegner, C. Im, A. Busing, and S. Heun, Efficient upconversion fluorescence in a blue-emitting spirobifluorene-anthracene copolymer doped with low concentrations of Pt(II)octaethylporphyrin, *J. Chem. Phys.* **123**, 074902 (2005).
- [8] V. Gray, D. Dzebo, M. Abrahamsson, B. Albinsson, and K. Moth-Poulsen, Triplet-triplet annihilation photon-upconversion: Towards solar energy applications, *Phys. Chem. Chem. Phys.* **16**, 10345 (2014).
- [9] N. Nishimura, V. Gray, J. R. Allardice, Z. Zhang, A. Pershin, D. Beljonne, and A. Rao, Photon upconversion from near-infrared to blue light with TIPS-anthracene as an efficient triplet-triplet annihilator, *ACS Mater. Lett.* **1**, 660 (2019).
- [10] T. F. Schulze and T. W. Schmidt, Photochemical upconversion: Present status and prospects for its application to solar energy conversion, *Energy Environ. Sci.* **8**, 103 (2015).
- [11] B. D. Ravetz, A. B. Pun, E. M. Churchill, D. N. Congreve, T. Rovis, and L. M. Campos, Photoredox catalysis using infrared light via triplet fusion upconversion, *Nature* **565**, 343 (2019).
- [12] M. P. Rauch and R. R. Knowles, Applications and prospects for triplet-triplet annihilation photon upconversion, *Chimia* **72**, 501 (2018).
- [13] S. H. Askes, A. Bahreman, and S. Bonnet, Activation of a photodissociative ruthenium complex by triplet-triplet annihilation upconversion in liposomes, *Angew. Chem. Int. Ed.* **53**, 1029 (2014).
- [14] Y. Sasaki, S. Amemori, H. Kouno, N. Yanai, and N. Kimizuka, Near infrared-to-blue photon upconversion by exploiting direct S-T absorption of a molecular sensitizer, *J. Mater. Chem. C* **5**, 5063 (2017).
- [15] M. Lebental, H. Choukri, S. Chénais, S. Forget, A. Siove, B. Geffroy, and E. Tutiš, Diffusion of triplet excitons in an operational organic light-emitting diode, *Phys. Rev. B.* **79**, 165318 (2009).
- [16] S. A. Bagnich and H. Bässler, Origin of delayed fluorescence of a ladder-type methyl-poly(para-phenylene) doped with Pt(II)octaethylporphyrin, *Chem. Phys. Lett.* **381**, 464 (2003).
- [17] Y. Zhang and S. R. Forrest, Triplet diffusion leads to triplet-triplet annihilation in organic phosphorescent emitters, *Chem. Phys. Lett.* **590**, 106 (2013).
- [18] S. T. Hoffmann, S. Athanasopoulos, D. Beljonne, H. Bässler, and A. Köhler, How do triplets and charges move in disordered organic semiconductors? A Monte Carlo study comprising the equilibrium and nonequilibrium regime, *J. Phys. Chem. C* **116**, 16371 (2012).
- [19] H. Bässler, Charge transport in disordered organic photoconductors a Monte Carlo simulation study, *Phys. Status Solidi B* **175**, 15 (1993).
- [20] A. Köhler and H. Bässler, Triplet states in organic semiconductors, *Mater. Sci. Eng., R* **66**, 71 (2009).
- [21] K. Masui, H. Nakanotani, and C. Adachi, Analysis of exciton annihilation in high-efficiency sky-blue organic

- light-emitting diodes with thermally activated delayed fluorescence, *Org. Electron.* **14**, 2721 (2013).
- [22] J. Popp, W. Kaiser, and A. Gagliardi, Impact of phosphorescent sensitizers and morphology on the photovoltaic performance in organic solar cells, *Adv. Theor. Simul.* **2**, 1800114 (2019).
- [23] C. Adachi and S. R. Forrest, Transient analysis of organic electrophosphorescence. II. Transient analysis of triplet-triplet annihilation, *Phys. Rev. B.* **62**, 10967 (2000).
- [24] N. C. Giebink and S. R. Forrest, Quantum efficiency roll-off at high brightness in fluorescent and phosphorescent organic light emitting diodes, *Phys. Rev. B.* **77**, 235215 (2008).
- [25] S. Reineke, K. Walzer, and K. Leo, Triplet-exciton quenching in organic phosphorescent light-emitting diodes with Ir-based emitters, *Phys. Rev. B.* **75**, 125328 (2007).
- [26] F. X. Zang, T. C. Sum, A. C. H. Huan, T. L. Li, W. L. Li, and F. Zhu, Reduced efficiency roll-off in phosphorescent organic light emitting diodes at ultrahigh current densities by suppression of triplet-polaron quenching, *Appl. Phys. Lett.* **93**, 023309 (2008).
- [27] S. M. Suresh, E. Duda, D. Hall, Z. Yao, S. Bagnich, A. M. Z. Slawin, H. Bassler, D. Beljonne, M. Buck, Y. Olivier, et al., A deep blue B,N-doped heptacene emitter that shows both thermally activated delayed fluorescence and delayed fluorescence by triplet-triplet annihilation, *J. Am. Chem. Soc.* **142**, 6588 (2020).
- [28] P. Y. Chou, H. H. Chou, Y. H. Chen, T. H. Su, C. Y. Liao, H. W. Lin, W. C. Lin, H. Y. Yen, I. C. Chen, and C. H. Cheng, Efficient delayed fluorescence via triplet-triplet annihilation for deep-blue electroluminescence, *Chem. Commun.* **50**, 6869 (2014).
- [29] F. B. Dias, Kinetics of thermal-assisted delayed fluorescence in blue organic emitters with large singlet-triplet energy gap, *Philos. Trans. R. Soc. London, Ser. A* **373**, 20140447 (2015).
- [30] S. T. Hoffmann, J. M. Koenen, U. Scherf, I. Bauer, P. Strohriegel, H. Bassler, and A. Kohler, Triplet-triplet annihilation in a series of poly(p-phenylene) derivatives, *J. Phys. Chem. B* **115**, 8417 (2011).
- [31] H. Goudarzi and P. E. Keivanidis, Triplet-triplet annihilation-induced up-converted delayed luminescence in solid-state organic composites: Monitoring low-energy photon up-conversion at low temperatures, *J. Phys. Chem. C* **118**, 14256 (2014).
- [32] A. Ligthart, X. de Vries, L. Zhang, M. C. W. M. Pols, P. A. Bobbert, H. van Eersel, and R. Coehoorn, Effect of triplet confinement on triplet-triplet annihilation in organic phosphorescent host-guest systems, *Adv. Funct. Mater.* **28**, 1804618 (2018).
- [33] S. Athanasopoulos, S. T. Hoffmann, H. Bassler, A. Kohler, and D. Beljonne, To hop or not to hop? understanding the temperature dependence of spectral diffusion in organic semiconductors, *J. Phys. Chem. Lett.* **4**, 1694 (2013).
- [34] I. I. Fishchuk, A. Kadashchuk, S. T. Hoffmann, S. Athanasopoulos, J. Genoe, H. Bassler, and A. Köhler, Unified description for hopping transport in organic semiconductors including both energetic disorder and polaronic contributions, *Phys. Rev. B.* **88**, 125202 (2013).
- [35] R. A. Marcus, Electron transfer reactions in chemistry. Theory and experiment, *Rev. Mod. Phys.* **65**, 599 (1993).
- [36] A. Miller and E. Abrahams, Impurity conduction at low concentrations, *Physical Review* **120**, 745 (1960).
- [37] A. Köhler and H. Bässler, What controls triplet exciton transfer in organic semiconductors?, *J. Mater. Chem.* **21**, 4003 (2011).
- [38] S. Athanasopoulos, E. Emelianova, A. B. Walker, and D. Beljonne, Modelling exciton diffusion in disordered conjugated polymers, *Proc. SPIE* **7722**, 772214 (2010).
- [39] S. Athanasopoulos, E. V. Emelianova, A. B. Walker, and D. Beljonne, Exciton diffusion in energetically disordered organic materials, *Phys. Rev. B.* **80**, 195209 (2009).
- [40] L. Zhang, H. van Eersel, P. A. Bobbert, and R. Coehoorn, Analysis of the phosphorescent dye concentration dependence of triplet-triplet annihilation in organic host-guest systems, *Chem. Phys. Lett.* **662**, 221 (2016).
- [41] L. Zhang, H. van Eersel, P. A. Bobbert, and R. Coehoorn, Clarifying the mechanism of triplet-triplet annihilation in phosphorescent organic host-guest systems: A combined experimental and simulation study, *Chem. Phys. Lett.* **652**, 142 (2016).
- [42] R. Coehoorn, P. A. Bobbert, and H. van Eersel, Effect of exciton diffusion on the triplet-triplet annihilation rate in organic semiconductor host-guest systems, *Phys. Rev. B.* **99**, 024201 (2019).
- [43] X. de Vries, P. Friederich, W. Wenzel, R. Coehoorn, and P. A. Bobbert, Triplet exciton diffusion in metalorganic phosphorescent host-guest systems from first principles, *Phys. Rev. B.* **99**, 205201 (2019).
- [44] See Supplemental Material at <http://link.aps.org/supplemental/10.1103/PhysRevApplied.14.034050> for additional simulation results, description of the effect of disorder on MA, and Marcus rates and expression of Pearson correlation function.
- [45] S. Athanasopoulos, E. Hennebicq, D. Beljonne, and A. B. Walker, Trap limited exciton transport conjugated polymers, *J. Phys. Chem. C* **112**, 11532 (2008).
- [46] P. Kordt, J. J. van der Holst, M. Al Helwi, W. Kowalsky, F. May, A. Badinski, C. Lennartz, and D. Andrienko, Modeling of organic light emitting diodes: From molecular to device properties, *Adv. Funct. Mater.* **25**, 1955 (2015).
- [47] H. T. Nicolai, M. Kuik, G. A. Wetzelaer, B. de Boer, C. Campbell, C. Risko, J. L. Bredas, and P. W. Blom, Unification of trap-limited electron transport in semiconducting polymers, *Nat. Mater.* **11**, 882 (2012).
- [48] B. Movaghar, M. Grunewald, B. Ries, H. Bassler, and D. Wurtz, Diffusion and relaxation of energy in disordered organic and inorganic materials, *Phys. Rev. B: Condens. Matter* **33**, 5545 (1986).
- [49] M. Ansari-Rad and S. Athanasopoulos, Theoretical study of equilibrium and nonequilibrium exciton dynamics in disordered semiconductors, *Phys. Rev. B.* **98**, 085204 (2018).
- [50] I. I. Fishchuk, A. Kadashchuk, L. Sudha Devi, P. Heremans, H. Bässler, and A. Köhler, Triplet energy transfer in conjugated polymers. II. A polaron theory description addressing the influence of disorder, *Phys. Rev. B.* **78**, 045211 (2008).
- [51] L. Grisanti, Y. Olivier, L. Wang, S. Athanasopoulos, J. Cornil, and D. Beljonne, Roles of local and nonlocal

- electron-phonon couplings in triplet exciton diffusion in the anthracene crystal, *Phys. Rev. B* **88**, 035450 (2013).
- [52] I. I. Fishchuk, A. Kadashchuk, S. T. Hoffmann, S. Athanopoulos, J. Genoe, H. Bässler, and A. Köhler, Analytic model of hopping transport in organic semiconductors including both energetic disorder and polaronic contributions, *AIP Conf. Proc.* **1610**, 47 (2014).
- [53] V. Arkhipov, E. Emelianova, G. Adriaenssens, and H. Bässler, Equilibrium carrier mobility in disordered organic semiconductors, *J. Non-Cryst. Solids* **299**, 1047 (2002).
- [54] J. J. M. van der Holst, M. A. Uijttewaal, B. Ramachandran, R. Coehoorn, P. A. Bobbert, G. A. de Wijs, and R. A. de Groot, Modeling and analysis of the three-dimensional current density in sandwich-type single-carrier devices of disordered organic semiconductors, *Phys. Rev. B* **79**, 085203 (2009).
- [55] Y. Shen and N. C. Giebink, Monte Carlo Simulations of Nanoscale Electrical Inhomogeneity in Organic Light-Emitting Diodes and its Impact on Their Efficiency and Lifetime, *Phys. Rev. Appl.* **4**, 054017 (2015).
- [56] D. T. Gillespie, A general method for numerically simulating the stochastic time evolution of coupled chemical reactions, *J. Comput. Phys.* **22**, 403 (1976).
- [57] R. Coehoorn and P. A. Bobbert, Effects of Gaussian disorder on charge carrier transport and recombination in organic semiconductors, *Phys. Status Solidi A* **209**, 2354 (2012).
- [58] I. Rörich, A.-K. Schönbein, D. K. Mangalore, A. Halda Ribeiro, C. Kasperek, C. Bauer, N. I. Crăciun, P. W. M. Blom, and C. Ramanan, Temperature dependence of the photo- and electroluminescence of poly(p-phenylene vinylene) based polymers, *J. Mater. Chem. C* **6**, 10569 (2018).
- [59] I. Rörich, O. V. Mikhnenko, D. Gehrig, P. W. Blom, and N. I. Craciun, Influence of energetic disorder on exciton lifetime and photoluminescence efficiency in conjugated polymers, *J. Phys. Chem. B* **121**, 1405 (2017).
- [60] S. T. Hoffmann, E. Scheler, J.-M. Koenen, M. Forster, U. Scherf, P. Strohriegel, H. Bässler, and A. Köhler, Triplet energy transfer in conjugated polymers. III. An experimental assessment regarding the influence of disorder on polaronic transport, *Phys. Rev. B* **81**, 165208 (2010).
- [61] X. de Vries, P. Friederich, W. Wenzel, R. Coehoorn, and P. A. Bobbert, Full quantum treatment of charge dynamics in amorphous molecular semiconductors, *Phys. Rev. B* **97**, 075203 (2018).